REMAINING USEFUL LIFE PREDICTIONS WITH DEEP LEARNING METHODS

(Final report)

Thomas Guillebot de Nerville*, Paul Strähle*, Anass Akrim†‡ and Rob Vingerhoeds†

*Institut Supérieur de l'Aéronautique et de l'Espace (ISAE-SUPAERO), Université de Toulouse, 31400 Toulouse, FRANCE
Email: {thomas.guillebot-de-nerville,paul.strahle}@student.isae-supaero.fr

†Institut Supérieur de l'Aéronautique et de l'Espace (ISAE-SUPAERO), Université de Toulouse, 31400 Toulouse, FRANCE
Email: {anass.akrim,rob.vingerhoeds}@isae-supaero.fr

‡Institut Clément Ader (UMR CNRS 5312) INSA/UPS/ISAE/Mines Albi, Université de Toulouse, 31400 Toulouse, FRANCE
Email: anass.akrim@univ-tlse3.fr

***Abstract*—This paper aims to compare Deep Learning models to predict the Remaining Useful Life (RUL) of a structure. These models are the following: the Convolutional Neural Network (CNN) family with a CNN and a Temporal Convolutional Network (TCN) architecture, the Recurrent Neural Networks (RNNs) family with a RNN, a Long short-term memorys (LSTMs) and a Gated Recurrent Units (GRUs) architecture.**

The dataset consists in simulations of the crack growth on plates, based on the Paris-Erdogan law. The training dataset is composed of 10,000 structures while the testing dataset is composed of 100 structures. Each architecture is optimized and trained on respectively 100, 500 and 1,000 structures from the training dataset. At the end, the different models are compared on their evaluation on the testing dataset, on the basis of a metric which is the accuracy in our case.

In order to optimize the architectures, a first step is to identify the fixed parameters, which do not have a significant impact on the accuracy, and the variable ones. The variable hyperparameters are optimized with a Random Search Strategy for 100 and 500 structures for the RNN family, the architure used for 1,000 structures being the one from the 500 structures optimization. For the CNN family, the variable hyperparameters are optimized for 100, 500 and 1,000 structures. The optimized models are then trained with an adaptative learning rate on the three numbers of structures. The results show that within the RNNs family, GRU gives the best result, while within the CNNs family, the TCN is the best model. Then, the results show that TCN gives a better performance than GRU with an accuracy reaching 99% for 1,000 structures.

I. Background

A. Deep Learning

In recent years Deep Learning, a subbranch of Machine Learning, has shown impressive results, especially in the fields of speech recognition, visual object recognition and object detection [1]. One requirement in using Deep Learning is the presence of sufficient amounts of data [2]. As more data becomes available in the engineering domain there is a recent surge of interest in using Deep Learning in engineering [3].

One of the strengths of Deep Learning approaches is their ability to deal with and detect complex relationships in large datasets [4]. This strength makes their usage also interesting in the Prognostics and Health Management (PHM) domain [5]. The potential of Deep Learning in PHM might not be fully exploited yet [6].

B. Prognostics and Health Management

According to Zio [7] PHM is a field of research and application which aims at making use of past, present and future information on the environmental, operational and usage conditions of a piece of equipment in order to detect its degradation, diagnose its faults, predict and proactively manage its failures. In the context of this project only the detection of degradation and prediction of failure are relevant.

PHM models can be divided into single and multi-model approaches. Multi-model approaches are a combination of different single-model approaches. Single-model approaches can be further divided into knowledge-based, data-driven and physics-based models. Within the data-driven models there are statistical, stochastic and Machine Learning models which is the category of Deep Learning models. [4]

II. Interest

Deep Learning has shown some impressive results when applied to RUL prediction as shown in [8]–[13] and other publications (For an overview see Akrim et al. [6]).

Within the available Deep Learning models there are two algorithms which are promising for RUL prediction: RNNs (Little [14] and Hopfield [15]) and CNNs (Lecun et al. [16]) [6].

RNNs are the common Deep Learning approach for time-dependent relationships and have therefore also achieved great interest in the PHM domain [6]. Pioneering models were developed such as Elman Recurrent Networks (ERMs) [17] or Jordan Networks [18], outperforming traditional Machine Learning Programs (MLPs) for sequence-prediction [6]. These algorithms were then widely explored by several researchers. Among them can be cited Yan et al. [19] for their work on material degradation evaluation and life prediction in 2007, and Kramti et al. [20] for having used ERMs for high-speed shaft bearing prognostics based on vibration signals [6].

An emerging type of Deep Learning network for time-dependent relationships are CNNs which might be able to outperform RNNs [21]. In one of the first applications of CNNs to PHM Li et al. suggested that CNNs can be used to obtain RUL prognoses for machinery [9]. The model was applied to the C-MAPSS dataset [22] and outperformed state-of-the-art prognostics approaches including RNN and LSTM models.

In this work a synthetic dataset is used as according to Fink et al. [23] the use of simulation environments and adaption to real-life applications is a promising future research approach as the data will more likely be sufficient in the source domain. The synthetic dataset used for this study aims at using this advantage.

The synthetic dataset matches strain gauge data to the RUL. The use of strain gauges as an input to an PHM model is interesting as they play a vital role in PHM in general [24] and specifically for the aircraft domain [25].

III. Aim

The goal of this study is to predict the RUL of precracked plates based on strain gauge measurements using Deep Learning. For the application of Deep Learning to crack growth for RUL prediction based on strain gauge measurements no results in the literature could be found. This study attempts to fill this research gap.

In a work done by Akrim [26] the Paris-Erdogan Law [27] was used to create a synthetic dataset of crack growth to train the model. The dataset consists of strain data from virtual strain gauges placed in the area around the crack and the corresponding RUL of the fuselage panels.

The Paris-Erdogan Law is applied to an infinite plate with a central horizontal crack. The strain gauges are placed in a 45°-Angle at the positions shown in Figure 1 relative to the center of the plate where the crack is located.

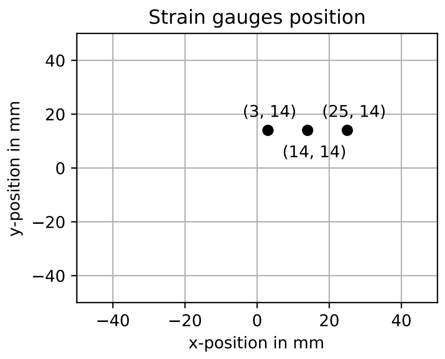

Fig. 1. Position of the strain gauges relative to the crack

The crack length in the Paris-Erdogan Law is a function of: k number of cylces, $\Delta\sigma$ stress range, m, C material constants, a_0 initial crack length. By calculating the crack growth until the crack length a reaches the critical crack length $a_{crit} = (\frac{K_{IC}}{\Delta\sigma\sqrt{\pi}})^2$ the simulation can determine the RUL for each simulated cycle. For the simulations the stress range $\Delta\sigma$ is kept constant while the initial crack length a_0 and the material parameters m and C are drawn from a normal distribution. 10000 structures are generated this way to form the training and validation dataset. For the testing dataset 100 structures are generated. The output of these simulations which form the input for the Deep Learning models is a table matching the strains from the strain gauges to the RUL calculated by the simulations. To reduce the dataset the results are only saved to the table every 500 cycles. Table I shows the structure of the generated training and validation dataset. The label ID denotes the specific structure.

TABLE I
Training and validation dataset structure

t	ID	$cycle$	ϵ_1	ϵ_2	ϵ_3	RUL_{bin}
1	1	0	$\epsilon_{1,1}$	$\epsilon_{2,1}$	$\epsilon_{3,1}$	$RUL_{bin,1}$
2	1	500	$\epsilon_{1,2}$	$\epsilon_{2,2}$	$\epsilon_{3,2}$	$RUL_{bin,2}$
3	1	1000	$\epsilon_{1,3}$	$\epsilon_{2,3}$	$\epsilon_{3,3}$	$RUL_{bin,3}$
4	1	1500	$\epsilon_{1,4}$	$\epsilon_{2,4}$	$\epsilon_{3,4}$	$RUL_{bin,4}$
$\vdots$	$\vdots$	$\vdots$	$\vdots$	$\vdots$	$\vdots$	$\vdots$
n	10000	$N_{f,10000}$	$\epsilon_{1,5}$	$\epsilon_{2,5}$	$\epsilon_{3,5}$	$RUL_{bin,5}$

The aim of this work is to predict the RUL based on current and past information from the 3 strain gauges using Deep Learning models. Different Deep Learning model architectures are to be used for that. The developed models must be trained and optimized before a comparison between them is made.

IV. Methods

A. Available Dataset

The provided datasets were separated into two distinguished parts, namely training and testing dataset. The first consists in 10 000 structures with different initial crack lengths. Most of the models were trained on this dataset using only a part of it, respectively 100, 500 and 1000 structures. While training, the last 100 structures of the training dataset were used as a validation dataset.

Then, the 100 structures from the second dataset were used to evaluate the performances of our models.

As it showed promising results in other applications of Deep Learning to PHM ([28], [29]), classification is an interesting alternative to regression for RUL prediction. Instead of trying to predict an exact RUL value the goal is to predict the correct RUL class with a lower and upper bound for the RUL. The generated dataset was composed of 80000 cycles at most. Therefore the chosen strategy has been to create 20 intervals following a parabolic equation (see Figure 2). The last of the 20 classes is for all RUL values greater than 80000 cycles.

To prepare the data as an input and output for the networks a sliding window approach is used. This approach maps the RUL at time t onto the current and past time steps of the input features $[x_{t-N+1}, x_{t-N+2}, ..., x_{t-1}, x_t]$ where N is the length of the sliding window. The resulting input matrix therefore has the dimension $(n-N) \times N \times k$ where n is the number of samples and k is the number of features. Figure 3 shows an

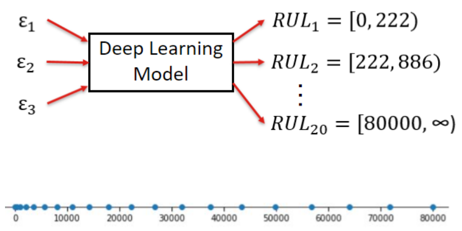

Fig. 2. RUL classification strategy

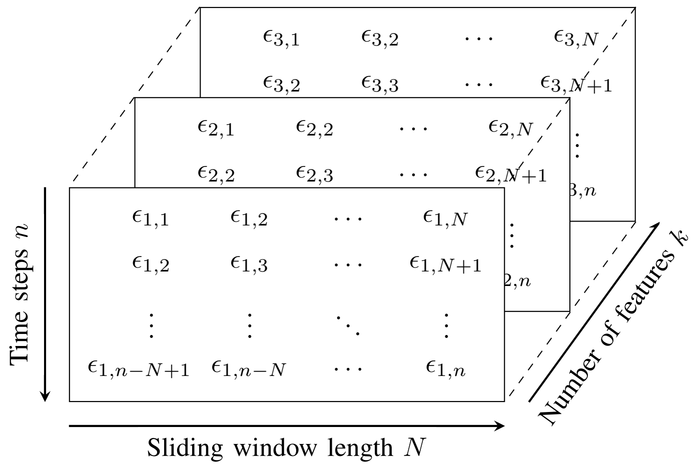

Fig. 3. Input matrix for the neural networks

example of how the time series data of the strain gauges from Table I is mapped to the input matrix.

The output matrix shown in Figure 4 is only one dimensional. It is only composed of the RUL bins which are mapped to the corresponding rows in the input matrix the dimension therefore is $(n - N)$.

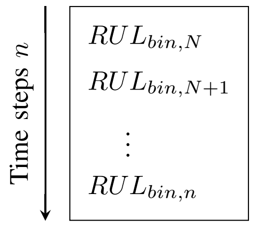

Fig. 4. Input matrix for the neural networks

As an input for the different models, datasets had to be normalized. While a specific layer was added at the beginning of CNN architectures to do so, the preprocessed data had to be normalized before being fed to the RNN models.

B. Recurrent Neural Networks

The common type of Deep Learning model for time series prediction are RNNs [21]. Due to their ability to store information within the cell, it can better remember information of time-dependant data.

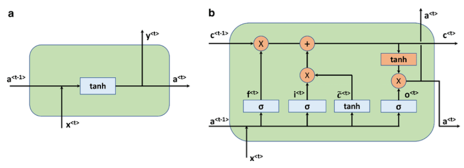

Fig. 5. RNN cell architecture. a. A simple RNN unit; b. an LSTM unit [30]

However, standard RNNs have some major drawbacks, such as the vanishing or exploding gradient problem, which limit their application [31]. LSTM networks (Hochreiter and Schmidhuber [32]) avoid this problem and have established themselves as one of the most used Deep Learning model types, especially for Natural Language Processing (NLP) [33]. For these reasons LSTMs will be one of the investigated RNN approaches in this project. Another investigated RNN approach is the GRUs. It is a simplified version of the LSTM. Due to this simplicity it has been gaining in popularity in recent years [34].

The key idea to GRU and LSTM is the memory cell which allows the network to remember information without much loss.

LSTM architecture consists in an input gate, a forget gate and an output gate. The input gate decides to add new information from the present input to the present cell state scaled by how much it wishes to add them. The forget gate allows the cell to know how to partially forget the previous cell state. Then, the output gate decides what to output from the new celle state.

For the GRU architecture, only two gates are implemented. The update gate decides the portion of updated candidate needed to calculate the current cell state, which in turn also decides the portion of the previous cell state retained. The relevance gate calculates how relevant the previous information is, and then is used in the candidate for the updated value.

Then, a simple RNN architecture will be explored to evaluate the possible benefits of more complex structures. An RNN unit only have a tanh layer after combining the cell state and the candidate.

C. Convolutional Neural Networks

Recent results suggest that CNNs can match or even outperform RNNs in time series related tasks [21]. The second major focus of this work are therefore CNN models.

The common CNN models deal with 2-Dimensional data as input such as pictures. The time sequence data used for PHM is in 1-Dimensional format. For this application 1D-CNN have been introduced. In the following this type of architecture is also called vanilla CNN. The key differences between them and the 2D-CNNs are that their input data is reduced by one dimension and the convolution filter only slides in one dimension [6]. Figure 6 shows an example of a simple CNN architecture with an illustration of the filter sliding over the time series.

Besides the general CNN architectures TCNs (Bai et al. [21]) are investigated in this work. A TCN is a specific CNN

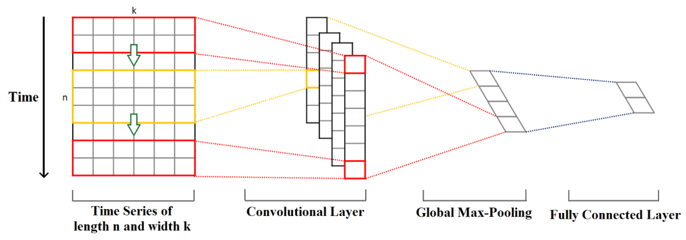

Fig. 6. Example of an 1D-CNN architecture [35]

architecture that tries to replicate some of the best practices for CNN architectures. As depicted in Fig. 7 a TCN is composed of multiple layers which include dilation. The dilation for each layer can be set arbitrarily but it is common practice to use multiples of 2 for it. Through dilation TCNs can increase their receptive field and therefore capture relationships over longer time sequences. One TCN layer is composed of a TCN residual block (see Figure 8 (a)). One block consists of two dilated convolutional layers. The activation function for the layers is always the ReLu function. The residual blocks include dropout and normalization layers between the convolutional layers. The blocks also include an optional skip connection with a 1x1 convolutional layer. Figure 8 (b) shows an exemplary TCN block with a kernel size of $k = 3$ and a dilation of $d = 1$. For more details on TCNs see [21].

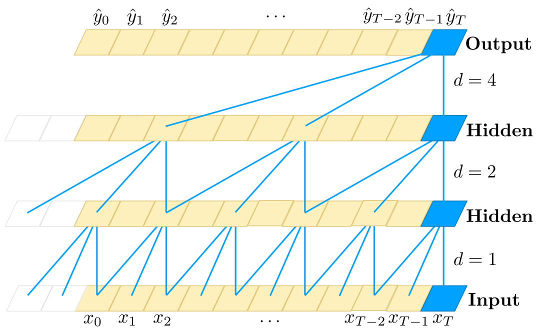
$\hat{y}_0$ $\hat{y}_1$ $\hat{y}_2$ ... $\hat{y}_{T-2}$ $\hat{y}_{T-1}$ $\hat{y}_T$
Output
$d = 4$
Hidden
$d = 2$
Hidden
$d = 1$
Input
x_0 x_1 x_2 ... x_{T-2} x_{T-1} x_T

Fig. 7. TCN with dilation factors d = 1; 2; 4 and filter size k = 3 [21]

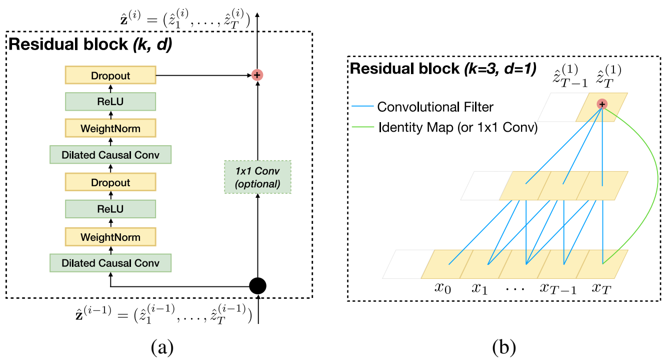
$\hat{\mathbf{z}}^{(i)} = (\hat{z}_1^{(i)}, \dots, \hat{z}_T^{(i)})$
Residual block (k, d)
Dropout
ReLU
WeightNorm
Dilated Causal Conv
Dropout
ReLU
WeightNorm
Dilated Causal Conv
1x1 Conv (optional)
$\hat{\mathbf{z}}^{(i-1)} = (\hat{z}_1^{(i-1)}, \dots, \hat{z}_T^{(i-1)})$
(a)
Residual block (k=3, d=1)
$\hat{z}_{T-1}^{(1)}$ $\hat{z}_T^{(1)}$
Convolutional Filter
Identity Map (or 1x1 Conv)
x_0 x_1 ... x_{T-1} x_T
(b)

Fig. 8. TCN block elements, (a): Generic TCN block, (b): Example for a TCN block [21]

D. Metric and loss function

To evaluate the performance of developed models a metric is needed. As the networks are used to perform classification instead of regression the accuracy metric is used. This metric calculates how many of the predictions made with the dataset are correct (e.g. the right RUL range is predicted)

$$Accuracy = \frac{Number\ of\ correct\ predictions}{Total\ number\ of\ predictions}. \tag{1}$$

This metric is applied during training and validation to compare different models against each other. The final assessment of the models is made by applying the accuracy metric to the testing dataset.

The used loss function which is used as the objective function for minimization by the backpropagation algorithm is the categorical crossentropy loss function

$$CE = -log(\frac{e^{s_p}}{\sum_j^C e^{s_j}}) \tag{2}$$

where s_j is the output of the network for Class j with s_p beeing the positive class.

E. Hyperparameter Optimization

To optimize the proposed network architectures a hyperparameter optimization is performed. The hyperparameters include the parameters for the training process (Learning rate and batch size), network parameters (Dropout rate, activation function etc.) and the network architecture itself (number of layers, size of the layers etc.).

There are different strategies for hyperparameter optimization which can be divided in Model-Free and Model-Based approaches. For this study only Model-Free approaches are considered as they are more common and easier to apply. The two common approaches are grid search and random search [36].

For grid search the user defines a discrete number of values for each parameter. The algorithm then tries out all possible combinations of these sets of values. This quickly leads to an excessive amount of training runs that need to be done as the number of possible combinations B grows exponentially with the dimensionality d of the search space. If the number of values per parameter is $n = 3$ and the dimensionality is just $d = 5$ the number of combinations already equals $B = n^d = 243$.

Random search works with a fixed number of evaluations where for each evaluation a value randomly is selected from a predefined set of values for each parameter. The set of values can either be continuous with a lower and upper bound for the values or a discrete set of predefined values. Random search works better than grid search when some parameters are more important than others, which is a property that holds true in many cases [36]. Figure 9 illustrates this property for one important and one unimportant parameter. With a fixed amount of B evaluations random search can evaluate up to B different values for each parameter. Whereas grid search is limited to $B^{1/N}$ values per parameter. It is expected that the networks in this study behave like most networks with regard to the varying importance of the hyperparameters and therefore random search is choosen for hyperparameter optimization.

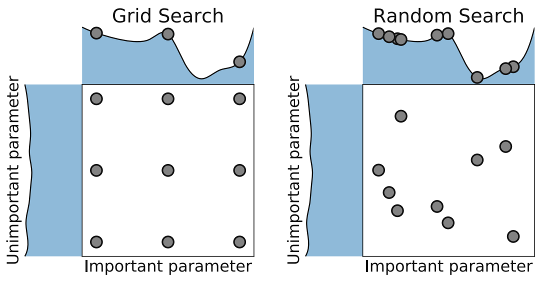

Fig. 9. Comparison of grid search and random search for an important and a unimportant parameter with 9 evaluations [36]

To select the best model after performing the hyperparameter optimization the accuracy of the model on the validation dataset is used.

F. Fine Tuning

After the optimum parameters for a model are found the model can be further improved by running more training epochs. To do so the models are trained with learning rate decay (lrDecay)). The best model from the hyperparameter optimization is taken and trained for a predefined number of epochs on the learning rate which was identified as the best one on the optimization. The learning rate is then lowered before the model is trained again for a fixed number of epochs. This step is repeated until convergence is achieved and no more significant improvements are visible. By using this approach the model in the early stages of training is less likely to get stuck in a local minimum and explores a wider range of possible configurations. As the training comes closer to an optimum the decaying learning rate helps with convergence and avoid oscillations. Besides this common beliefs there are probably more reasons to the effectiveness of lrDecay). According to You et al. [37] is the initially large learning rate preventing the network from memorizing noisy data while the decaying learning rate helps with learning complex patterns in the dataset.

V. Results

A. Model architectures

All RNNs architectures were based on the same template. The dataset being normalized before being fed to the models, there were no need for a specific layer of normalization. A flexible number of layers were implemented in the networks, as well as the number of cells in each layer, scaled by a power of 2. A possible dropout and recurrent dropout could also be added for each layer. At the end of the architecture, a dense layer with 20 units were added in order to match the number of RUL classes $C = 20$.

Based on the CNN architecture of Li et al. [9] which was used for aero-engine RUL prediction a vanilla CNN architecture is generated. The first layer of the architecture is for layer normalization. Afterwards a flexible number of 1D-convolutional layers is added which all have the same number of filters and an identical kernel size. The output of the convolutional layers is flattened before the final dense output layer which has 20 nodes to match the number of RUL classes $C = 20$. As an example Figure 10 shows the final architecture after the hyperparameter optimization with 1000 training structures.

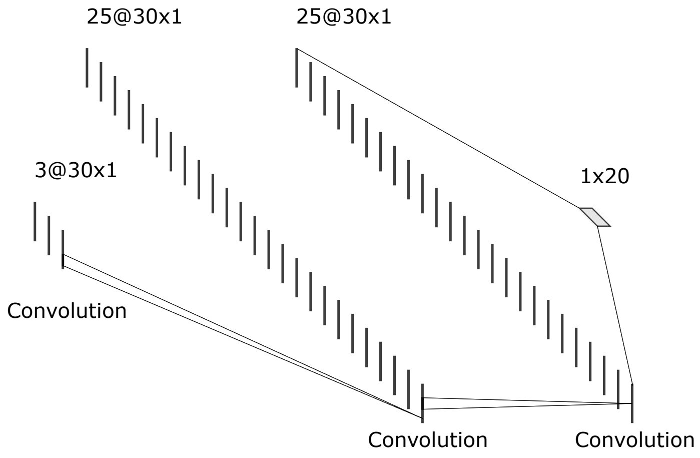

Fig. 10. CNN architecture after hyperparameter optimization with 1000 training structures

A TCN architecture template is generated based on the results of Liu et al. [10] who used the network for RUL prediction of roller bearings. The architecture consists of multiple TCN residual blocks with a dilation increasing with multiples of 2 with the first layer having a dilation of $d = 1$. Each block features the same number of filters with an identical kernel size. The next layer after the TCN blocks is the dense output layer which has 20 nodes to match the number of RUL classes $C = 20$. The skip connection layer is activated for all residual blocks.

B. Hyperparameter optimization

The hyperparameter optimization is performed using random search as described in IV. The used training dataset consists of 100, 500 or 1000 structures. For validation always 100 structures different to the training structures are used. The model selection is based on the accuracy of the models on the validation dataset. Not all available parameters of the networks are considered for the optimization as that would increase the computational effort drastically. The reduction also helps to shift the focus of the optimization on the important parameters and avoid varying parameters which have no or only little influence on the accuracy of the network.

1) RNN, LSTM and GRU hyperparameters optimization: Following the same method used for the CNN and TCN hyperparameter optimization, fixed parameters were previously set for each architecture, to avoid searching for hyperparameters which would not be relevant in the accuracy improvement.

Those fixed parameters are the same for the RNN, LSTM and GRU architectures, and can be found in Table II.

TABLE II
FIXED PARAMETERS FOR RNN HYPERPARAMETERS OPTIMIZATION

Parameter	Value
Batch size	4096
Activation function	ReLU
Epochs	500
Sequence length	30

Once those parameters fixed, usefull hyperparameters were identified. These are the ones which can have a significant impact on accuracy improvement. They were identified on 100 structures, and then reused for 500 structures. Due to a lack of time, only the best architecture identified from the optimization on 500 structures was used to train on 1000 structures, and then evaluate the performance. It appeared that the variable hyperparameters to try were the same for RNN, LSTM and GRU. They can be found in Table III.

TABLE III
VARIABLE PARAMETERS FOR VANILLA CNN HYPERPARAMETER OPTIMIZATION

Parameter	Value set
Number of hidden layers	$\{1, 2, 3\}$
Number of cells per layer	$\{32, 64, 128, 256\}$
Dropout rate	$\{0, 0.1\}$
Recurrent Dropout rate	$\{0, 0.1\}$
Learning rate	$\{10^{-2}, 10^{-3}\}$

The Random Search strategy were then used to optimize those hyperparameters on 100 structures and 500 structures, with a fixed sliding window size of 30. The learning rate is not reported for the Fine Tuning will use an adaptative Learning Rate strategy to optimize the performance of the final training. The results of hyperparameters optimization can be found in Table IV for both RNN, LSTM and GRU.

TABLE IV
RESULTS OF THE HYPERPARAMETERS OPTIMIZATION FOR 100 AND 500 STRUCTURES

Training structures	100			500		
Type of architecture	RNN	LSTM	GRU	RNN	LSTM	GRU
Number of hidden layers	3	2	3	3	2	2
Number of cells per layer	32	64	256	32	128	256
Dropout rate	0	0	0	0	0	0
Recurrent Dropout rate	0	0	0	0	0	0
Validation accuracy	0.752	0.688	0.726	0.871	0.700	0.819

It then can be then understood that RNNs do not need many layers to get a good accuracy compared to CNN. The best accuracy can be found with no more than 2 or 3 layers in this case. Indeed, too many layers and cells for this amount of data might lead the model to lose itself, along with the fact that the computational time increases drastically. The Dropout and Recurrent Dropout rates were optimized at 0% meaning that the models did not overfit for this range of structures. This result is better visible as the validation accuracy follows the training accuracy on the Fine Tuning in Figure 17, 18 and 19.

2) Vanilla CNN and TCN hyperparameters optimization: Table V lists the fixed parameters of the vanilla CNN optimization. The sliding window length includes multiple values as the influence of that parameter is studied by performing multiple optimization runs with different lengths of the sliding window.

TABLE V
FIXED PARAMETERS FOR VANILLA CNN HYPERPARAMETER OPTIMIZATION

Parameter	Value
Batch size	4096
Sliding window length	$\{5, 10, 15, 20, 30, 40\}$
Activation function	ReLU
Padding	Padding with zeros
Dropout	No dropout

Table VI lists the variable parameters and their set of possible values for the CNN hyperparameter optimization. The chosen range for the parameters is the result of a preliminary analysis to identify meaningful boundaries for them.

TABLE VI
VARIABLE PARAMETERS FOR VANILLA CNN HYPERPARAMETER OPTIMIZATION

Parameter	Value set
Number of convolutional layers	$\{2, 4, 6, 8\}$
Number of filters per layer	$\{15, 20, 25, 30, 35, 40, 45, 50\}$
Kernel size	$\{3, 6, 9, 12\}$
Learning rate	$\{10^{-2}, 10^{-3}\}$

For the vanilla CNN the hyperparameter optimization is performed on 100, 500 and 1000 training structures. For the smallest dataset of 100 structures the optimization is performed on the full range of different sliding window lengths as listed in Table VI. The optimizations on 500 and 1000 structures are only performed with a sliding window size of $N = 30$. All optimization runs are performed for 500 training epochs and with a total of $B = 100$ evaluations.

Figure 11 shows the achieved maximum validation accuracy after the hyperparameter optimization for different lengths of the sliding window. The accuracy increases approximately linearly with size of the sliding window although the absolute value of the improvement remains relatively small. The size of the sliding window can not be increased above a size of 40 as then the sliding window would be larger than the timeseries of some of the structures. A too big sliding window besides that has the disadvantage that it can only be applied if data is already collected for at least as many timesteps as the sliding window requires. This means that there could be situations in which the first predictions can only be made just before the part fails or in the worst case after it fails. As a result of these considerations and the neglectible difference between the sliding window sizes of 30 and 40 a size of $N = 30$ is choosen for all further hyperparameter optimizations runs with the vanilla CNN on 500 and 1000 structures.

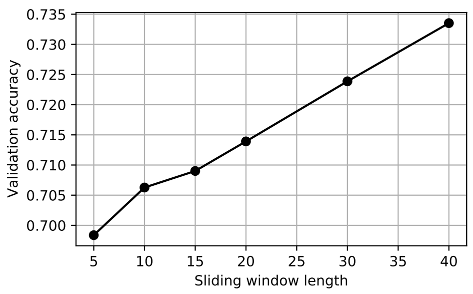

Fig. 11. Vanilla CNN hyperparameter optimization for different sliding window sizes for training on 100 structures

Table VII shows the different architectures from the hyperparameter optimization that achieved the best results with the respective sliding window length on 100 training structures. There is no clear trend for the network architecture in relation to the sliding window size. This is backed by the fact that the 2nd and 3rd best networks for each respective hyperparameter optimization can have significantly different architectures to the best one. This observation leads to the conclusion that there are many different network architectures that can give equal results.

TABLE VII
BEST MODELS OF THE VANILLA CNN HYPERPARAMETER OPTIMIZATION FOR DIFFERENT SLIDING WINDOW LENGTHS WITH TRAINING ON 100 STRUCTURES

Sliding window size	5	10	15	20	30	40
Number of convolutional layers	4	2	4	2	6	6
Number of filters per layer	25	35	30	45	20	20
Kernel size	3	6	9	9	6	3
Learning rate	10^{-2}	10^{-2}	10^{-2}	10^{-2}	10^{-2}	10^{-2}
Validation accuracy	0.698	0.706	0.709	0.714	0.724	0.734

Figure 12 shows the history of the training and validation accuracy for some of the different sliding window sizes for the training with 100 structures. There is little to no overfitting on the training dataset for all of the shown training runs. The 500 training epochs lead to a sufficient convergence for all the runs.

The hyperparameter optimizations of the vanilla CNN with 500 training structures and a sliding window size of 30 leads to an improvement of the validation accuracy. Showing that the network architecture if provided with more data can better learn the relationships within the dataset. An increase of the training dataset to 1000 structures leads to further improvement. This is a result of the lower learning rate of this network which has not fully converged yet (see Figure 13) Table VIII depicts the best network architecture with the achieved validation accuracy for 100, 500 and 1000 training structures with a sliding window size of 30. There is no clear trend visible in the network architectures indicating that there are many different possible architectures which achieve the same results. This hypothesis is supported by some of the

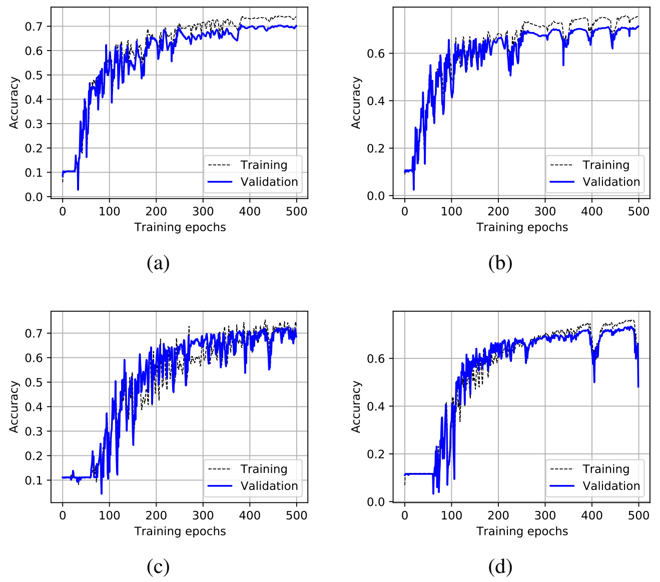

Fig. 12. Training and validation accuracy history for the best model of the vanilla CNN hyperparameter optimization on 100 training structures with a sliding window size of: (a): 10, (b): 20, (c): 30, (d): 40

other architectures created by the hyperparameter optimization which achieve similar results with distinctly different architectures.

TABLE VIII
BEST MODELS OF THE VANILLA CNN HYPERPARAMETER OPTIMIZATION FOR 100, 500 AND 1000 TRAINING STRUCTURES

Training structures	100	500	1000
Sliding window size		30	
Number of convolutional layers	6	2	4
Number of filters per layer	20	40	25
Kernel size	6	12	9
Learning rate	10^{-2}	10^{-2}	10^{-3}
Validation accuracy	0.724	0.788	0.789

Figure 13 shows the training history for the best models of the vanilla CNN hyperparameter optimization when training on 500 and 1000 structures respectively. None of the two models shows significant overfitting on the training dataset. Both models are not yet fully converged and therfore have room for improvement. This potential is exploited in the model fine tuning in section XXX. The training history of the model trained on 500 epochs shows an instability at around 480 epochs. Indicating that the learning rate should be reduced which is done in the subsequent model fine tuning.

Table IX lists the fixed parameters of the TCN optimization. The sliding window length includes multiple values as the influence of that parameter is studied by performing multiple optimization runs with different lengths of the sliding window.

Table X lists the variable parameters and their set of possible values for the TCN hyperparameter optimization. The chosen range for the parameters is the result of a preliminary analysis

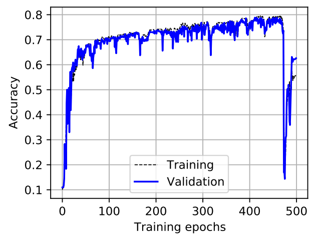

(a)

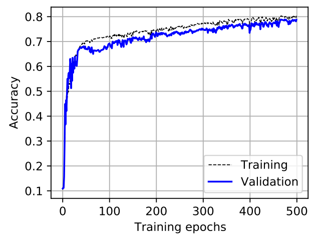

(b)

Fig. 13. Training and validation accuracy history for the best model of the vanilla CNN hyperparameter optimization on (a): 500 and (b): 1000 training structures

TABLE IX
FIXED PARAMETERS FOR TCN HYPERPARAMETER OPTIMIZATION

Parameter	Value
Batch size	4096
Sliding window length	$\{10, 15, 20, 30\}$
Activation function	ReLU
Padding	Causal padding
Normalization	Weight normalization

to identify meaningful boundaries for them. The indicated number of layers directly corresponds the the maximum dilation as the dilations rises with multiples of two for each TCN block. For e.g. 4 blocks the dilation in the blocks is $[1, 2, 4, 8]$.

TABLE X
VARIABLE PARAMETERS FOR TCN HYPERPARAMETER OPTIMIZATION

Parameter	Value set
Number of layers	$\{4, 6, 8, 10\}$
Number of filters per layer	$\{15, 20, 25, 30, 35, 40, 45, 50\}$
Kernel size	$\{3, 6, 9, 12\}$
Dropout rate	$\{0.0, 0.1, 0.2\}$
Learning rate	$\{10^{-2}, 10^{-3}\}$

As for the vanilla CNN the hyperparameter optimization for the TCN is performed on 100, 500 and 1000 training structures. For the smallest dataset of 100 structures the optimization is performed on the full range of different sliding window lengths as listed in Table VI. The optimizations on 500 and 1000 structures are only performed with a sliding window size of $N = 30$. All optimization runs are performed for 500 training epochs and with a total of $B = 50$ evaluations. The evaluations are reduced compared to the CNN optimization because of the increased computational effort for the TCN.

Figure 14 shows the achieved maximum validation accuracy after the hyperparameter optimization for different lengths of the sliding window. There is a significant increase of the accuracy between a length of 15 and 30. The other differences seem to be the result of scatter as a result of the training as well as the random search which does lead to different network architectures in each optimization run. To keep a big enough distance to the drop in the accuarcy for windows sizes ≤ 20 a sliding window size of $N = 30$ is chosen for all further hyperparameter optimizations with the TCN on 500 and 1000 structures.

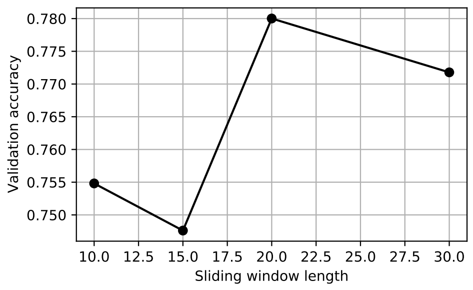

Fig. 14. TCN hyperparameter optimization for different sliding window sizes for training on 100 structures

Figure 12 shows the history of the training and validation accuracy for different sliding window sizes for the training with 100 structures. There is little to no overfitting on the training dataset for all of the training runs. The 500 training epochs lead to a sufficient convergence for all the runs.

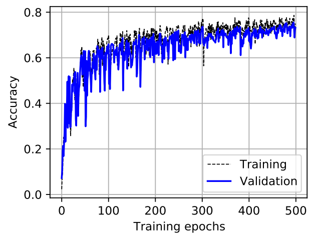

(a)

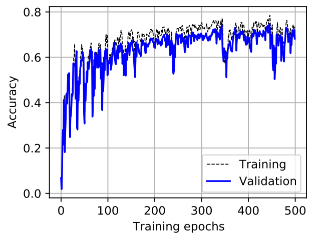

(b)

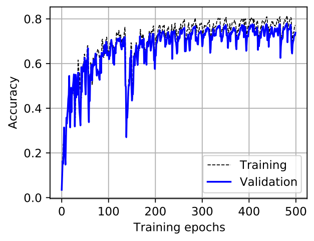

(c)

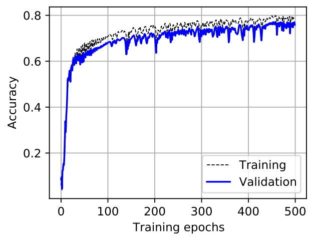

(d)

Fig. 15. Training and validation accuracy history for the best model of the TCN hyperparameter optimization on 100 training structures with a sliding window size of: (a): 10, (b): 15, (c): 20, (d): 30

Performing the hyperparameter optimization of the TCN with 500 and 1000 structures respectively leads to significant improvements of the validation accuracy. This indicates that the network is able to better learn the relations in the dataset when feed with more data. Table XI depicts the best network architecture with the achieved validation accuracy for 100, 500 and 1000 training structures with a sliding window size of 30. The network architectures are very similar which shows that independent of the used training dataset a similar architecture works best.

Figure 13 shows the training history for the best models of the vanilla CNN hyperparameter optimization when training on 500 and 1000 structures respectively. None of the two

TABLE XI

BEST MODELS OF THE TCN HYPERPARAMETER OPTIMIZATION FOR 100, 500 AND 1000 TRAINING STRUCTURES

Training structures	100	500	1000
Sliding window size		30	
Number of convolutional layers	8	8	8
Number of filters per layer	30	25	35
Kernel size	2	2	2
Dropout rate	0.0	0.0	0.0
Learning rate	10^{-3}	10^{-2}	10^{-2}
Validation accuracy	0.772	0.883	0.908

models shows significant overfitting on the training dataset. Both models are not yet fully converged and therfore have room for improvement. This potential is exploited in the model fine tuning in section XXX. The training history of the model trained on 500 epochs shows an instability at around 480 epochs. Indicating that the learning rate should be reduced which is done in the subsequent model fine tuning.

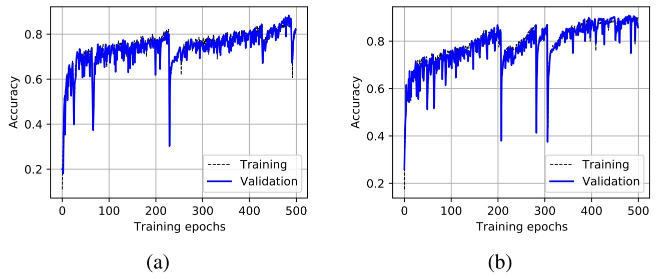

Fig. 16. Training and validation accuracy history for the best model of the TCN hyperparameter optimization on (a): 500 and (b): 1000 training structures

C. Fine Tuning

As the hyperparameters were optimized, the resulting models had to be trained with an adaptative learning rate to optimize their performance. The models are further refined on the same dataset on which the optimization was performed. lrDecay) starts with a learning rate of 10^{-2} or 10^{-3} depending on which value was choosen in the hyperparameter optimization, decreasing to 10^{-3}, 10^{-4} and then 10^{-5}. With each learning rate, models were trained on a maximum of 500 epochs which leads to a training with a maximum of 2000 epochs. After the fine tuning the models are tested on the testing dataset to evaluate their final performance.

1) RNN, LSTM and GRU fine tuning: For the RNN, LSTM and GRU the results for the history of the training can be found groupes by the number of structures in Figures 17, 18 and 19. It can be clearly observed that the adaptative learning rate strategy allows a better training for each model. Once the models trained, they were evaluated on the testing dataset. All the results for the validation accuracy and the testing accuracy can be found in Table XII.

It can be observed little to no overfitting in each training. In addition, some training history show an unstable improvement,

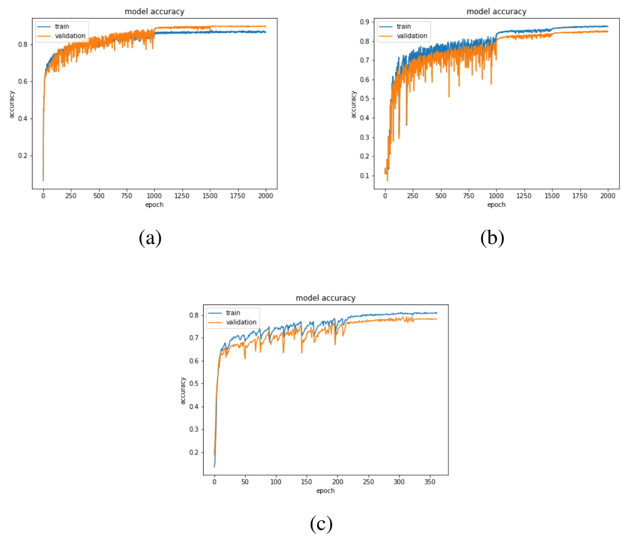

Fig. 17. Training and validation accuracy for 100 training structures with lrDecay): (a): RNN, (b): LSTM, (c): GRU

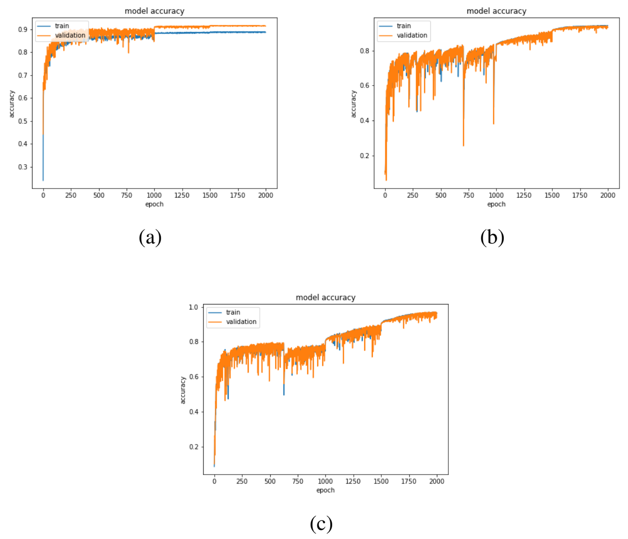

Fig. 18. Training and validation accuracy for 500 training structures with lrDecay): (a): RNN, (b): LSTM, (c): GRU

with even a decreasing accuracy for some learning rates. This could have an impact on the final accuracy. Nevertheless, it seems that decreasing the learning rate improves the stability of the training.

Regarding the final validation and testing accuracies, there is a significant difference between 100 and 500 structures. The different models increased both their validation and testing accuracies, even though the differences between 500 and 1000 structures are less notable. The best improvement is noticed with GRU, reaching 97% for the validation accuracy for 1000 structures.

However, a huge difference is observed between the validation and the testing accuracy. This could be due to the metric

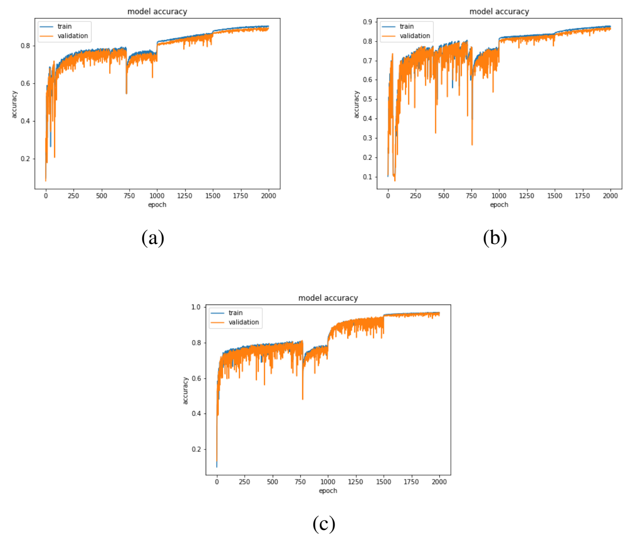

Fig. 19. Training and validation accuracy for 1000 training structures with lrDecay): (a): RNN, (b): LSTM, (c): GRU

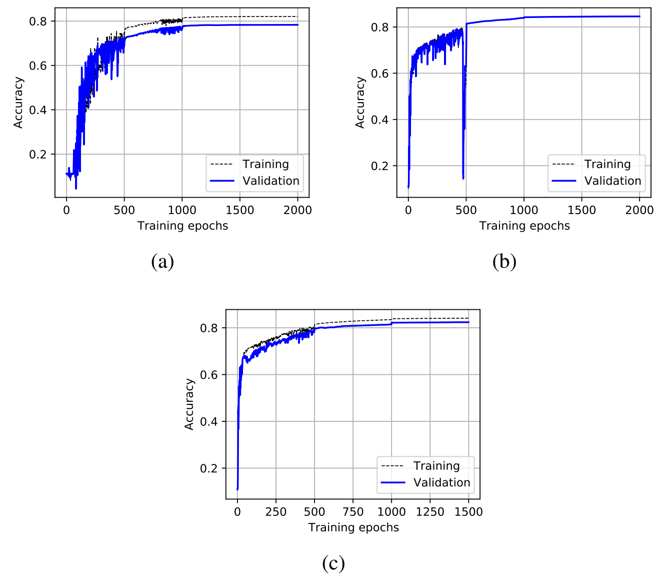

Fig. 20. Training and validation accuracy history for the best models of the vanilla CNN hyperparameter optimization on (a): 100, (b): 500 and (c): 1000 structures after fine tuning the models with lrDecay) on the same datasets

used. As the scaling for the classification follows a parabolic equation, the first classes are narrower than the last classes. Studying the distribution of the different RUL to predict in the testing dataset might show that they are more present in the first classes than for the training dataset, which is then more difficult to predict. A possible solution might be then to choose another metric which would take into account this distribution of the RUL classes.

2) Vanilla CNN and TCN fine tuning: For each of the best identified network architectures of the vanilla CNN and TCN hyperparameter optimizations further training with lrDecay) is performed to improve the performance. For the models which were optimized on 100 structures the models with a sliding window length of 30 are choosen for futher refinement.

Figure 20 depicts the training history for the fine tuning on 100, 500 and 1000 structures. The networks show little to no overfitting on the training dataset. There is steady improvement of the accuracy towards convergence except for the training on 500 structures which shows a steep drop at around 500 epochs.

The training historys of the TCN fine tuning can be seen in Figure 21. The best model from the hyperparameter optimization on 1000 structures was not only fine tuned on 1000 structures but also on the full dataset of 9900 structures to see if any improvements can be realised (see Figure 21 (d)). During the first phase of training with the highest learning rate there are strong oscillations for all the models. The decrease of the learning rate helps to stabilize the training and for all the models gives a significant rise to the accuracy. In the later stages of the training all the models show a stable convergence. Only the model trained on 100 structures shows a bit of overfitting on the training dataset while the other models show no such signs.

3) Model comparison: As a final validation all the fine tuned models are tested with the testing dataset of 100 struc-

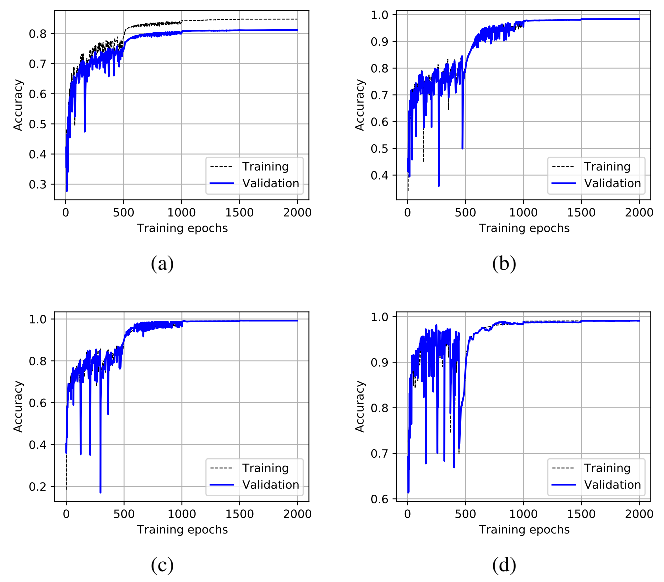

Fig. 21. Training and validation accuracy history for the best models of the TCN hyperparameter optimization on (a): 100, (b): 500, (c): 1000 and (c): 9900 structures after fine tuning the models with lrDecay) on the same datasets

tures. Table XII shows an overview of the achieved accuracy for all RNN (Vanilla RNN, LSTM and GRU) and CNN models (Vanilla CNNs and TCNs).

It can be noticed that for RNNs models, the difference between the validation accuracy and the testing accuracy is notable. The networks have difficulties to generalize the patterns learned to new sets of data. But, as previously analysed, this could be also the classification scaling which gives a larger bandwith on the last classes, while the testing dataset might focus more on the first classes, which are smaller. This leads to an increasing possibilty of wrong prediction of the RUL on the testing dataset. One lead to explore would be then to adapt the metric to take into account this evolution of the classes bandwidth. Nonetheless, GRUs seem to work better for the validation accuracy on larger datasets, reaching 97% on 1000 structures.

For the vanilla CNN and TCN models there is a steady increase in the achieved accuracy on the testing set if the amount of structures for training is increased. The increase in testing accuracy corresponds largely to the increase in validation accuracy. The testing accuracy is in the same order of magnitude as the validation accuracy indicating that the networks generalize well to new sets of data. In general TCNs work better than CNNs especially on the larger datasets of 500 and 1000 structures where the TCN achieves close to 100% accuracy. When trained on the complete dataset the TCN achieved 100% accuracy on the testing dataset.

TABLE XII
ACCURACY OF ALL FINE TUNED RNN (VANILLA RNN, LSTM AND GRU) AND CNN MODELS (VANILLA CNNS AND TCNS) ON THE VALIDATION AND TESTING DATASETS

Model type	Vanilla CNN			TCN			
Number of training structures	100	500	1000	100	500	1000	10000
Validation accuracy	0.78	0.84	0.82	0.81	0.98	0.99	0.99
Testing accuracy	0.82	0.84	0.84	0.82	0.98	0.99	1.00

Model type	Vanilla RNN			LSTM			GRU		
Number of training structures	100	500	1000	100	500	1000	100	500	1000
Validation accuracy	0.899	0.914	0.891	0.850	0.932	0.932	0.783	0.964	0.970
Testing accuracy	0.84	0.90	0.78	0.73	0.83	0.72	0.70	0.77	0.75

VI. CONCLUSIONS

All chosen models could successfully be trained on the available dataset and achieve an accuracy of at least 70% on the testing dataset. It usually was the case that more available training data leads to a better performance of the models. The best performance in general was achieved by TCN models. Confirming the recent results of other researchers like Bai et al. **"cite –Bai2018"** and Li et al. [9]. This again questions the general practice to use RNN models as a standard for time series prediction while CNN models should be used for image classification. The TCN models when trained on more than 500 structures achieved closed to 100% accuracy confirming their excellent suitability to time series prediction problems. Thus, a lead to explore would be a hybrid model between an GRU and a TCN architecture, to improve the different patterns to learn in the data.

The good results achieved on this dataset should come at no surprise as the dataset is synthetic without the flaws of real world data. There is no noise in the data which would never be the case in reality. The virtual strain gauges are always placed at the exact same location while in reality there is always a position tolerance when placing them on a structure.

REFERENCES

[1] Y. LeCun, Y. Bengio, and G. Hinton, "Deep learning," *Nature*, vol. 521, no. 7553, pp. 436–444, 2015, ISSN: 1476-4687. DOI: 10.1038/nature14539.

[2] J. Z. Sikorska, M. Hodkiewicz, and L. Ma, "Prognostic modelling options for remaining useful life estimation by industry," *Mechanical Systems and Signal Processing*, vol. 25, no. 5, pp. 1803–1836, 2011, ISSN: 0888-3270. DOI: 10.1016/j.ymssp.2010.11.018. [Online]. Available: https://www.sciencedirect.com/science/article/pii/S0888327010004218.

[3] A. Voulodimos, N. Doulamis, G. Bebis, and T. Stathaki, "Recent developments in deep learning for engineering applications," *Computational Intelligence and Neuroscience*, vol. 2018, p. 8 141 259, 2018, ISSN: 1687-5265. DOI: 10.1155/2018/8141259.

[4] J. J. Montero Jimenez, S. Schwartz, R. Vingerhoeds, B. Grabot, and M. Salaün, "Towards multi-model approaches to predictive maintenance: A systematic literature survey on diagnostics and prognostics," *Journal of Manufacturing Systems*, vol. 56, pp. 539–557, 2020, ISSN: 0278-6125. DOI: 10.1016/j.jmsy.2020.07.008. [Online]. Available: https://www.sciencedirect.com/science/article/pii/S0278612520301187.

[5] S. Wu, K. L. Tsui, N. Chen, Q. Zhou, Y. Hai, and W. Wang, "Prognostics and health management: A review on data driven approaches," *Mathematical Problems in Engineering*, vol. 2015, p. 793 161, 2015, ISSN: 1024-123X. DOI: 10.1155/2015/793161.

[6] A. Akrim, C. Gogua, R. Vingerhoeds, and M. Salaun, "Review of prognostics approaches with a particularfocus on the current machine learning algorithms," 2021.

[7] E. Zio, "Prognostics and Health Management of Industrial Equipment," in *Diagnostics and Prognostics of Engineering Systems: Methods and Techniques*, S. Kadry, Ed., ISBN13: 9781466620957, IGI Global, Sep. 2012, pp. 333–356. DOI: 10.4018/978-1-4666-2095-7.ch017. [Online]. Available: https://hal-supelec.archives-ouvertes.fr/hal-00778377.

[8] L. Xu, S. F. Yuan, J. Chen, and Q. Bao, "Deep learning based fatigue crack diagnosis of aircraft structures," in *7th Asia-Pacific Workshop on Structural Health Monitoring*, 2018. [Online]. Available: https://www.ndt.net/search/docs.php3?id=24093.

[9] X. Li, Q. Ding, and J.-Q. Sun, "Remaining useful life estimation in prognostics using deep convolution neural networks," *Reliability Engineering & System Safety*, vol. 172, pp. 1–11, 2018, ISSN: 0951-8320. DOI: 10.1016/j.ress.2017.11.021. [Online]. Available: https://www.sciencedirect.com/science/article/pii/S0951832017307779.

[10] C. Liu, L. Zhang, and C. Wu, "Direct remaining useful life prediction for rolling bearing using temporal convolutional networks," (Dec. 6, 2019), Xiamen, China: IEEE, Dec. 6, 2019, pp. 2965–2971, ISBN: 978-1-7281-2486-5. DOI: 10.1109/SSCI44817.2019.9003163.

[11] M. Yuan, Y. Wu, and L. Lin, "Fault diagnosis and remaining useful life estimation of aero engine using lstm neural network," in *2016 IEEE International Conference on Aircraft Utility Systems (AUS)*, 2016, pp. 135–140. DOI: 10.1109/AUS.2016.7748035.

[12] Y. Wu, M. Yuan, S. Dong, L. Lin, and Y. Liu, "Remaining useful life estimation of engineered systems using vanilla lstm neural networks," *Neurocomputing*, vol. 275, pp. 167–179, 2018, ISSN: 0925-2312. DOI: 10.1016/j.neucom.2017.05.063. [Online]. Available: https://www.sciencedirect.com/science/article/pii/S0925231217309505.

[13] K. Park, Y. Choi, W. Choi, H.-Y. Ryu, and H. Kim, "Lstm-based battery remaining useful life prediction with multi-channel charging profiles," *IEEE Access*, vol. PP, pp. 1–1, Jan. 2020. DOI: 10.1109/ACCESS.2020.2968939.

[14] W. A. Little, "The existence of persistent states in the brain," in *From High-Temperature Superconductivity to Microminiature Refrigeration*, B. Cabrera, H. Gutfreund, and V. Kresin, Eds. Boston, MA: Springer US, 1996, pp. 145–164, ISBN: 978-1-4613-0411-1. DOI: 10.1007/978-1-4613-0411-1_12.

[15] J. J. Hopfield, "Neural networks and physical systems with emergent collective computational abilities," *Proceedings of the National Academy of Sciences*, vol. 79, no. 8, pp. 2554–2558, 1982, ISSN: 0027-8424. DOI: 10.1073/pnas.79.8.2554. eprint: https://www.pnas.org/content/79/8/2554.full.pdf. [Online]. Available: https://www.pnas.org/content/79/8/2554.

[16] Y. Lecun, L. Bottou, Y. Bengio, and P. Haffner, "Gradient-based learning applied to document recognition," *Proceedings of the IEEE*, vol. 86, no. 11, pp. 2278–2324, 1998. DOI: 10.1109/5.726791.

[17] J. L. Elman, "Finding structure in time," *Cognitive Science*, vol. 14, no. 2, pp. 179–211, 1990, ISSN: 0364-0213. DOI: 10.1016/0364-0213(90)90002-E. [Online]. Available: https://www.sciencedirect.com/science/article/pii/036402139090002E.

[18] M. I. Jordan, "Chapter 25 - serial order: A parallel distributed processing approach," in *Neural-Network Models of Cognition*, ser. Advances in Psychology, J. W. Donahoe and V. Packard Dorsel, Eds., vol. 121, North-Holland, 1997, pp. 471–495. DOI: 10.1016/S0166-4115(97)80111-2. [Online]. Available: https://www.sciencedirect.com/science/article/pii/S0166411597801112.

[19] J. Yan and P. Wang, "Blade material fatigue assessment using elman neural networks," vol. 2007, Jan. 2007. DOI: 10.1115/IMECE2007-43311.

[20] S. E. Kramti, J. Ben Ali, L. Saidi, M. Sayadi, and E. Bechhoefer, "Direct wind turbine drivetrain prognosis approach using elman neural network," in *2018 5th International Conference on Control, Decision and*

Information Technologies (CoDIT), 2018, pp. 859–864. DOI: 10.1109/CoDIT.2018.8394926.

[21] S. Bai, J. Z. Kolter, and V. Koltun, "An empirical evaluation of generic convolutional and recurrent networks for sequence modeling," *CoRR*, vol. abs/1803.01271, 2018. arXiv: 1803.01271. [Online]. Available: http://arxiv.org/abs/1803.01271.

[22] A. Saxena, K. Goebel, D. Simon, and N. Eklund, "Damage propagation modeling for aircraft engine run-to-failure simulation," in *2008 International Conference on Prognostics and Health Management*, 2008, pp. 1–9. DOI: 10.1109/PHM.2008.4711414.

[23] O. Fink, Q. Wang, M. Svensén, P. Dersin, W.-J. Lee, and M. Ducoffe, "Potential, challenges and future directions for deep learning in prognostics and health management applications," *Engineering Applications of Artificial Intelligence*, vol. 92, p. 103 678, 2020, ISSN: 0952-1976. DOI: 10.1016/j.engappai.2020.103678. [Online]. Available: https://www.sciencedirect.com/science/article/pii/S0952197620301184.

[24] T. Tinga and R. Loendersloot, "Physical model-based prognostics and health monitoring to enable predictive maintenance," in *Predictive Maintenance in Dynamic Systems: Advanced Methods, Decision Support Tools and Real-World Applications*, E. Lughofer and M. Sayed-Mouchaweh, Eds. Cham: Springer International Publishing, 2019, pp. 313–353, ISBN: 978-3-030-05645-2. DOI: 10.1007/978-3-030-05645-2_11.

[25] F. Timothy, M. Devinder, and H. Iain, "F-35 joint strike fighter structural prognosis and health management an overview," Jan. 2009. DOI: 10.1007/978-90-481-2746-7_68.

[26] A. Akrim, "Description algorithm."

[27] P. Paris and F. Erdogan, "A critical analysis of crack propagation laws," *Journal of Basic Engineering*, vol. 85, no. 4, pp. 528–533, Dec. 1963. DOI: 10.1115/1.3656900.

[28] C.-L. Liu, W.-H. Hsaio, and Y.-C. Tu, "Time series classification with multivariate convolutional neural network," *IEEE Transactions on Industrial Electronics*, vol. 66, no. 6, pp. 4788–4797, Dec. 6, 2019. DOI: 10.1109/TIE.2018.2864702.

[29] W. Xiao, "A probabilistic machine learning approach to detect industrial plant faults," Mar. 2016. arXiv: 1603.05770 `[stat.ML]`.

[30] G. Chen, "Recurrent neural networks (rnns) learn the constitutive law of viscoelasticity," *Computational Mechanics*, vol. 67, Mar. 2021. DOI: 10.1007/s00466-021-01981-y.

[31] Y. Bengio, P. Simard, and P. Frasconi, "Learning long-term dependencies with gradient descent is difficult.," eng, *IEEE transactions on neural networks*, vol. 5, pp. 157–66, 2 1994. DOI: 10.1109/72.279181.

[32] S. Hochreiter and J. Schmidhuber, "Long Short-Term Memory," *Neural Computation*, vol. 9, no. 8, pp. 1735–1780, Nov. 1997, ISSN: 0899-7667. DOI: 10.1162/neco.1997.9.8.1735. eprint: https://direct.mit.edu/neco/article-pdf/9/8/1735/813796/neco.1997.9.8.1735.pdf.

[33] Y. Wu, M. Schuster, Z. Chen, *et al.*, "Google's neural machine translation system: Bridging the gap between human and machine translation," Sep. 2016. arXiv: 1609.08144 `[cs.CL]`.

[34] R. Rana, "Gated recurrent unit (gru) for emotion classification from noisy speech," Dec. 2016. arXiv: 1612.07778 `[cs.HC]`.

[35] R. A. Sayyad, "How to use convolutional neural networks for time series classification," *Medium*, [Online]. Available: https://medium.com/@Rehan_Sayyad/how-to-use-convolutional-neural-networks-for-time-series-classification-80575131a474.

[36] M. Feurer and F. Hutter, "Hyperparameter optimization," in *Automated Machine Learning*, Springer, Cham, 2019, pp. 3–33.

[37] K. You, M. Long, J. Wang, and M. I. Jordan, *How does learning rate decay help modern neural networks?* 2019. arXiv: 1908.01878 `[cs.LG]`.